ELSEVIER

Colloids and Surfaces
A: Physicochemical and Engineering Aspects 121 (1997) 189–202

COLLOIDS AND SURFACES A

Modeling colloid transport and deposition in saturated fractures

Constantinos V. Chrysikopoulos *, Assem Abdel-Salam

Department of Civil and Environmental Engineering, University of California, Irvine, CA 92697, USA

Received 19 July 1996; accepted 19 November 1996

Abstract

A model is developed to describe the transport of colloids in a saturated fracture with a spatially variable aperture, accounting for colloid deposition onto fracture surfaces under various physicochemical conditions. The fracture plane is partitioned into unit elements with different apertures generated stochastically from a log-normal distribution. The model also accounts for colloid size exclusion from fracture elements with small apertures. Both equilibrium and kinetic colloid deposition onto fracture surfaces are investigated. Colloid surface exclusion is incorporated in the dynamics of kinetic deposition. The impact of deposited colloids on further colloid deposition is described by either a linear or a non-linear blocking function. The resulting system of governing partial differential equations is solved numerically using the fully implicit finite difference method. Model simulations illustrate the presence of preferential colloid transport in the fracture plane. It is shown that size exclusion increases the dispersion of colloids and leads to earlier breakthrough, especially for large-size particles. Furthermore, it is demonstrated that surface exclusion enhances colloid transport, and the assumption of clean-bed media may underestimate liquid-phase colloid concentrations.

Keywords: Colloid deposition; Colloid transport; Saturated fractures; Size exclusion; Spatially variable aperture; Stochastic modeling

1. Introduction

The transport of natural colloids in subsurface environmental systems under various geochemical conditions has recently received considerable attention [1,5,20,21,35,38,39,42,43,47], because some colloidal particles (e.g. viruses, bacteria, radiocolloids) can cause serious environmental hazards. Moreover, there is substantial evidence from both laboratory and field experiments that contaminants can sorb on the surface of colloidal particles [9,27,45,52,53], because colloids have a high surface-area to volume ratio and compete with formation surfaces for contaminant sorption. Therefore, the association of contaminants with mobile colloidal particles may influence and possibly enhance the rate of contaminant transport [2,3,15,18,26,28,29].

Colloids represent a class of very fine particles which generally range in size from 1 nm to 10 μm [10]; their name is derived from the Greek word "κόλλα", meaning "glue" [34]. Colloids present in subsurface formations are mainly mineral particles in the form of metal oxides, humic macromolecules, bacteria and viruses [49]. In fractured media, colloids are formed by the microerosion of minerals present in the subsurface matrix as a result of formation crushing due to tectonic activity [12]. Colloidal particles are also produced by the mechanical action of infiltrating water and

* Corresponding author.

PII S0927-7757(96)03979-9

chemical dissolution of rock matrix minerals. In addition, colloids form by changes in groundwater geochemical conditions such as pH, major element composition, redox potential, or partial pressures of CO_2 [24].

The transport of colloids in fractured subsurface media is considerably controlled by colloid deposition onto formation surfaces. At the microscopic scale, colloid deposition is governed by several collision and attachment mechanisms. The collision mechanisms are Brownian diffusion, interception and sedimentation. However, for particles smaller than 1 μm in diameter, collision is dominated by Brownian diffusion. Attachment mechanisms are mainly dominated by repulsive electrostatic, attractive van der Waals, and hydrodynamic forces [25,50]. Numerous studies on colloid deposition in porous and fractured media have examined deposition mechanisms at the microscopic scale (i.e. at the particle–sorbent scale) [4,8] and the laboratory scale (i.e. at the experimental column scale) [6,22,33,52].

Colloid deposition onto fracture surfaces can be characterized by either equilibrium or kinetic relationships. For mathematical simplicity, many models for colloid transport in porous and fractured media incorporate a reversible, equilibrium-deposition expression [10,14,23,44,51]. Kinetic colloid deposition models are based on the assumption that deposited colloids form either a monolayer coverage on the sorbent's surface when interparticle electrostatic forces prohibit contact of colloids [4], or a multilayer coverage when attractive electrostatic surface forces enhance particle–particle interactions [37]. It should be noted, however, that charged colloidal particles may cover less surface area of a sorbent than uncharged particles, because the presence of intercolloidal forces hinder physical contact or overlapping between particles [5].

Previous research publications on colloid transport in saturated, fractured media accounted for colloid deposition but have not explored surface exclusion effects in conjunction with colloid size exclusion from portions of fractures with small apertures. In this work, we formulate a mathematical model describing colloid transport and deposition in a large fracture with a spatially variable aperture. The impact of some important equilibrium and kinetic colloid deposition mechanisms on colloid transport is investigated. In order to make the problem tractable, some of the deposition mechanisms are incorporated into the transport model as lumped parameters. The fracture aperture is treated as a stochastic variable, and the resulting set of coupled partial differential equations is solved numerically. The effect of colloid penetration into the rock matrix surrounding the fracture has been investigated extensively in earlier studies [1,18], and is not included in the present work.

2. Model development

2.1. Governing transport and flow equations

The governing partial differential equation for colloid transport in a two-dimensional fracture with spatially variable aperture, assuming that colloids are stable of equal size and may deposit onto fracture surfaces but do not penetrate the rock matrix surrounding the fracture, is given by [3]:

$$b(x,y)\frac{\partial n(t,x,y)}{\partial t}+2\frac{\partial n^*(t,x,y)}{\partial t} = \nabla\cdot[b(x,y)\boldsymbol{D}\cdot\nabla n(t,x,y)-b(x,y)\boldsymbol{U}n(t,x,y)] \quad (1)$$

where b is the fracture aperture, n is the concentration of colloids suspended in the liquid phase, n^* is the concentration of colloids deposited onto fracture surfaces expressed as the mass of colloids per unit area of the fracture surface, x is the coordinate along the fracture length, y is the coordinate along the fracture width, t is time, ∇ is the two-dimensional vector operator (del), $\nabla\cdot$ denotes divergence, $\boldsymbol{U}=(U_x,U_y)^T$ is a two-dimensional interstitial fluid velocity vector (where U_x and U_y are the components of the interstitial velocity in the x and y directions, respectively, and the exponent T denotes transpose), and $\boldsymbol{D}$ is a 2×2 symmetric matrix of hydrodynamic dispersion coefficients, which can be determined from the velocity field by employing the following

expression [7]:

$$D_{ij}(x,y)=\alpha_T\delta_{ij}|U|+(\alpha_L-\alpha_T)\frac{U_i(x,y)U_j(x,y)}{|U|}+\mathscr{D} \tag{2}$$

where α_L and α_T are the longitudinal and transverse dispersivities in the x and y directions, respectively, δ_{ij} is the Kronecker delta ($\delta_{ij}=0$ for $i\neq j$ and $\delta_{ij}=1$ for $i=j$) with subscripts $ij=xx$, xy, yx or yy, $\mathscr{D}$ is the Brownian diffusion coefficient for colloids, and $|U|=(U_x^2+U_y^2)^{1/2}$ is the magnitude of the interstitial velocity vector. The velocity vector is two-dimensional because fracture-aperture variability leads to a non-uniform velocity field. The governing transport equation (Eq. (1)) does not account for colloid diffusion into the rock matrix surrounding the fracture. It should be noted, however, that colloid penetration into the rock matrix simply leads to a decrease in the liquid-phase colloid concentration in the fracture, and has been thoroughly investigated elsewhere [1]. The initial and boundary conditions imposed on the two-dimensional fracture for the colloid transport model are:

$$n(0,x,y)=0 \tag{3a}$$

$$n(t,0,y)=n_0 \tag{3b}$$

$$\frac{\partial n(t,l_x,y)}{\partial x}=0 \tag{3c}$$

$$-D_{yy}(x,0)\frac{\partial n(t,x,0)}{\partial y}+U_y(x,0)n(t,x,0)=0 \tag{3d}$$

$$-D_{yy}(x,l_y)\frac{\partial n(t,x,l_y)}{\partial y}+U_y(x,l_y)n(t,x,l_y)=0 \tag{3e}$$

where l_x and l_y are the fracture dimensions in the x and y directions, respectively, and n_0 is the constant colloid concentration at the source. Eq. (3a) establishes that there is no initial concentration of colloids suspended in the liquid phase. The constant concentration boundary condition (Eq. (3b)) implies colloid concentration continuity at the upstream boundary. Eq. (3c) imposes the condition that the dispersive flux of colloids is zero and that concentration continuity is preserved at the downstream boundary. Furthermore, Eq. (3d) and Eq. (3e) imply that the lower and upper boundaries of the two-dimensional fracture are impervious to advective as well as dispersive transport of colloids.

The velocity components in the x and y directions at any location within the fracture are obtained by [11]:

$$U_x(x,y)=-K_f(x,y)\frac{\partial h(x,y)}{\partial x}=-\frac{\gamma b^2(x,y)}{12\mu}\frac{\partial h(x,y)}{\partial x} \tag{4}$$

$$U_y(x,y)=-K_f(x,y)\frac{\partial h(x,y)}{\partial y}=-\frac{\gamma b^2(x,y)}{12\mu}\frac{\partial h(x,y)}{\partial y} \tag{5}$$

where h is the total head potential, $K_f=\gamma b^2/12\mu$ is the hydraulic conductivity of the fracture, γ is the specific weight of the interstitial fluid, and μ is the dynamic viscosity of the interstitial fluid. The distribution of the total head potential within the fracture is obtained by the following steady-state partial differential equation describing fluid flow in a fracture with a spatially variable aperture:

$$\frac{\partial}{\partial x}\left[b^3(x,y)\frac{\partial h(x,y)}{\partial x}\right]+\frac{\partial}{\partial y}\left[b^3(x,y)\frac{\partial h(x,y)}{\partial x}\right]=0 \tag{6}$$

Eq. (6) was derived by Abdel-Salam and Chrysikopoulos [3] from mass-balance considerations over a fixed control fracture volume, and is a valid approximation when the curvature of the fracture is small [32]. The boundary conditions imposed on the two-dimensional fracture for the interstitial fluid flow model are:

$$\frac{\partial h(t,x,0)}{\partial y}=0 \tag{7a}$$

$$\frac{\partial h(t,x,l_y)}{\partial y}=0 \tag{7b}$$

$$h(t,0,y)=h_0 \tag{7c}$$

$$h(t,l_x,y)=0 \tag{7d}$$

where h_0 is a constant total head potential. Eq. (7a) and Eq. (7b) represent the no-flow top and bottom

boundaries, respectively, whereas Eq. (7c) and Eq. (7d) represent the constant head left (upstream) and right (downstream) boundaries, respectively (for the physical orientation of the fracture, see Fig. 1). The direction of the flow is from left to right. It should be noted that both the governing colloid transport equation (Eq. (1)) and the interstitial fluid flow equation (Eq. (6)) are stochastic partial differential equations because b is a stochastic variable.

2.2. Equilibrium colloid deposition

For the case where colloids deposit onto fracture surfaces relatively quickly compared to groundwater velocity, the deposition process can be described by the following linear local equilibrium relationship:

$$n^*(t,x,y) = Kn(t,x,y) \tag{8}$$

where K is the partition coefficient for colloid deposition onto fracture surfaces. Equilibrium deposition is reversible and may lead to a dense coverage of the fracture's surfaces. It should be noted, however, that Eq. (8) does not account for surface exclusion effects.

2.3. Kinetic colloid deposition

For time-dependent colloid deposition in a saturated fracture, under the assumption that the colloid filtration theory [16] is applicable, the following kinetic deposition model can be used:

$$\frac{\partial n^*(t,x,y)}{\partial t} = r_f \frac{n(t,x,y)}{b(x,y)} - r_r n^*(t,x,y) \tag{9}$$

where r_f and r_r are the forward and reverse colloid deposition rate coefficients, respectively. The forward rate coefficient is defined as:

$$r_f = \kappa (U_x^2 + U_y^2)^{1/2} F(n^*) \tag{10}$$

where κ is the colloid deposition coefficient, depending on several physicochemical properties of particles and collectors as well as on microscopic colloid-deposition mechanisms (i.e. Brownian diffusion, van der Waals and electrostatic forces), and $F(n^*)$ is the dynamic blocking function (DBF), which takes into account the effect of previously deposited particles on subsequent colloid deposition by specifying the portion of the fracture surface area available for deposition (surface exclusion effect). The DBF depends on the shape and size of the colloids, the geometry of

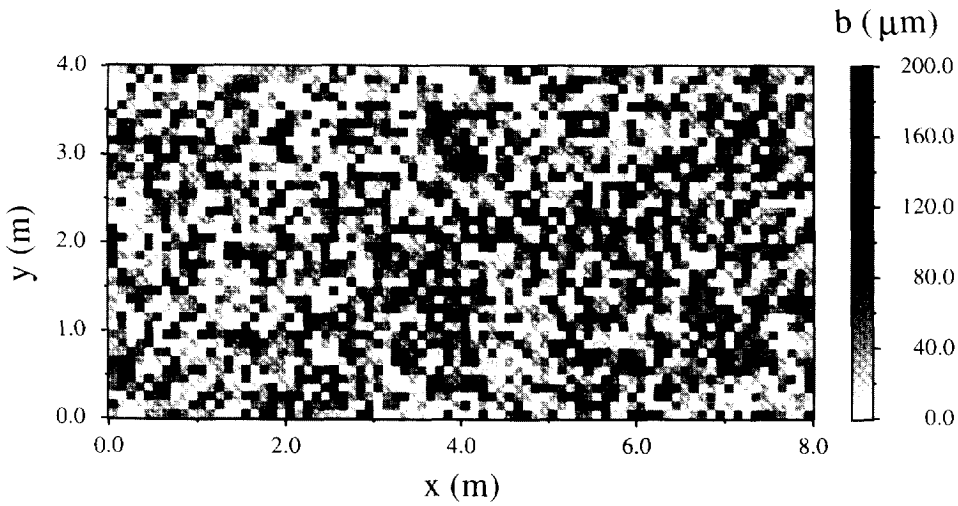

Fig. 1. Schematic illustration of the physical system modeled. The fracture is partitioned into 80 × 40 equal-size elements. The gray scale represents aperture sizes.

sorbent, flow characteristics, and the physicochemical properties of the interstitial fluid. The value of the DBF ranges between 1 for a fracture surface free of colloids ($n^*=0$) and 0 for a fracture surface completely covered (monolayer) by deposited colloids ($n^*=n^*_{max}$, where n^*_{max} is the maximum deposited colloid concentration). A linear (Langmuirian) DBF as well as several non-linear DBFs have been proposed in the literature for a variety of physical systems.

The colloid deposition coefficient κ presented in the expression describing the forward rate coefficient (Eq. (10)) can be approximated for cases of ideal flow conditions and collectors of regular geometrical shape (i.e. rotating disk, spherical and cylindrical collectors, a plate in a uniform flow, parallel-plate channel, and continuous moving surfaces) [13,53]. For natural subsurface formations, or for the fracture with a spatially variable aperture considered in this work, the mechanisms controlling the colloid deposition coefficient are, in general, very complex and depend on the nature of the collector surface. Any kind of surface roughness or spatial variability of the surface charge can substantially affect colloid deposition. Because of inadequate information to predict in advance colloid deposition onto the fracture walls, in this work the deposition coefficient is considered a lumped parameter. Furthermore, it should be noted that the term "dynamic blocking function" was introduced by Johnson and Elimelech [19] in a one-dimensional model describing the transport of monodisperse colloids through a packed column of spherical collectors, thus building upon the pioneering work of Adamczyk and co-workers [4,5], who used the term "blocking parameter" in analyzing colloid surface-coverage rates.

2.3.1. Linear (Langmuirian) DBF

The Langmuirian dynamic blocking function, which is linearly dependent on colloid surface coverage, has been used by many investigators [31,36,38,47] and is expressed as follows:

$$F(n^*)=\frac{\epsilon_{max}-\epsilon}{\epsilon_{max}} \tag{11}$$

where ϵ and ϵ_{max} are the fraction and maximum fraction of a sorbent surface covered (blocked) by deposited colloids, respectively. It should be noted that ϵ_{max} corresponds to the maximum deposited colloid concentration (n^*_{max}), which is a function of colloidal particle size and available sites for colloid deposition. The preceding relationship incorporates blocking effects due to physical coverage of the sorbent's surface area by previously deposited colloids, as well as for possible additional inhibition of subsequent colloid deposition (blocking greater than the projected or cross-sectional area of the deposited colloid) due to energy barriers created by electrostatic repulsive forces originating from charged, deposited colloids.

2.3.2. Non-linear DBF

Schaaf and Talbot [41] developed a DBF based on the random sequential adsorption (RSA) process, which is governed by irreversible deposition without surface diffusion and colloidal particle overlapping (i.e. monolayer coverage). The RSA DBF was derived by considering the probability of a spherical particle to deposit on a flat surface with previously deposited particles present, and is valid only for uncharged colloidal particles at the maximum surface coverage possible of $\epsilon_{max}=0.546$. An improved, more flexible version of this DBF was presented by Adamczyk et al. [4], and is given as:

$$F(n^*)=1-2.184\left[\frac{\epsilon}{\epsilon_{max}}\right]+0.986\left[\frac{\epsilon}{\epsilon_{max}}\right]^2+0.229\left[\frac{\epsilon}{\epsilon_{max}}\right]^3 \tag{12}$$

Eq. (12) is a non-linear function of the colloid surface coverage, and is valid for charged colloidal particles and any surface coverage up to $0.8\epsilon_{max}$. For higher surface coverage, the following relationship can be used [30]:

$$F(n^*)=\frac{(\epsilon_{max}-\epsilon)^3}{2k^2} \tag{13}$$

where k is an empirical parameter dependent on the area blocked by a single deposited particle.

2.3.3. Deposition model parameter estimation

In order to estimate the portion of a fracture surface area covered by colloids (ϵ), the number of deposited particles per unit surface area of the fracture (N^*) is obtained from the deposited colloid concentration (n^*) by the following expression:

$$N^*(t,x,y)=\frac{n^*(t,x,y)}{\rho_p V_p}=\frac{6n^*(t,x,y)}{\rho_p \pi d_p^3} \tag{14}$$

where ρ_p is the colloidal particle density, $V_p=\pi d_p^3/6$ is the volume of a spherical colloidal particle, and d_p is the diameter of a colloidal particle. Eq. (14) transforms the deposited mass concentration to particle number concentration. The maximum number of particles which can possibly deposit on a fracture surface area is defined by:

$$N^*_{max}=\frac{1}{\alpha} \tag{15}$$

where α is the area of the fracture surface blocked by a deposited colloidal particle. The parameter α is proportional to the projected (cross-sectional) area of a colloidal particle ($A_p=\pi d_p^2/4$), and is given by

$$\alpha=\beta A_p=\beta\left(\frac{\pi d_p^2}{4}\right) \tag{16}$$

where β is the excluded area factor, which is a dimensionless parameter representing the ratio of the fracture surface area blocked by a deposited colloidal particle to the projected area of the particle ($\beta\geq 1$ and $\alpha\geq A_p$). It should be noted, however, that the term "excluded area factor" is equivalent to the term "dimensionless area blocked" defined by Song and Elimelech (Eq. (41) in Ref. [46]), or to the term "excluded area parameter" employed by Johnson and Elimelech [19]. In view of Eqs. (14)–(16), the portion of a fracture surface area blocked by colloids is evaluated as:

$$\epsilon(t,x,y)=\frac{A_p N^*(t,x,y)}{\alpha N^*_{max}}=\frac{3}{2}\frac{n^*(t,x,y)}{\rho_p d_p} \tag{17}$$

The maximum fraction of a fracture surface area blocked by deposited colloids is obtained by replacing N^* with N^*_{max} in Eq. (17) to yield:

$$\epsilon_{max}=\frac{A_p}{\alpha}=\frac{1}{\beta} \tag{18}$$

where the latter formulation in Eq. (18) is the consequence of employing the definition of α (see Eq. (16)).

3. Methodology

The two-dimensional fracture considered in this study is illustrated in Fig. 1. The fracture plane is partitioned into 80×40 equal-size unit elements in the x and y directions, respectively. Each element exhibits a constant aperture. The aperture field in the fracture is generated stochastically by the geostatistical code COVAR [54]. It is assumed that the aperture distribution in the fracture plane follows a log-normal distribution with a mean of 1.65 μm and a standard deviation of 0.45 μm, and varies spatially according to an isotropic exponential autocovariance function with correlation length of 0.3 m.

For each realization of the aperture field, the distribution of the total head potential (h) within the fracture is obtained by solving the governing fluid flow equation (Eq. (6)) subject to Eqs. (7a), (7b), (7c) and (7d) using the central finite differences approximation as outlined by Huyakorn and Pinder [17] and Strikwerda [48]. The constant head potential in the upstream boundary condition (Eq. (7c)) is set to $h_0=1.0\times 10^{-4}$ m. Subsequently, the velocity components at each unit element of the fracture plane are obtained from Eq. (4) and Eq. (5) with $\gamma=9.778\times 10^6\ \mathrm{g\,m^{-2}\,s^{-2}}$ and $\mu=0.8904\ \mathrm{g\,m^{-1}\,s^{-1}}$. The corresponding hydrodynamic dispersion coefficients at each unit element are estimated by employing Eq. (2) with the assumption that $\alpha_L=0.01$ m, $\alpha_T=0.001$ m, and $\mathscr{D}$ is negligible.

Colloid-transport model simulations are conducted for several colloid deposition conditions under the assumption that the colloidal particles are spherical and of identical size. Furthermore, colloids are expected to follow the least-resistance flowpath, thus bypassing areas in the fracture with

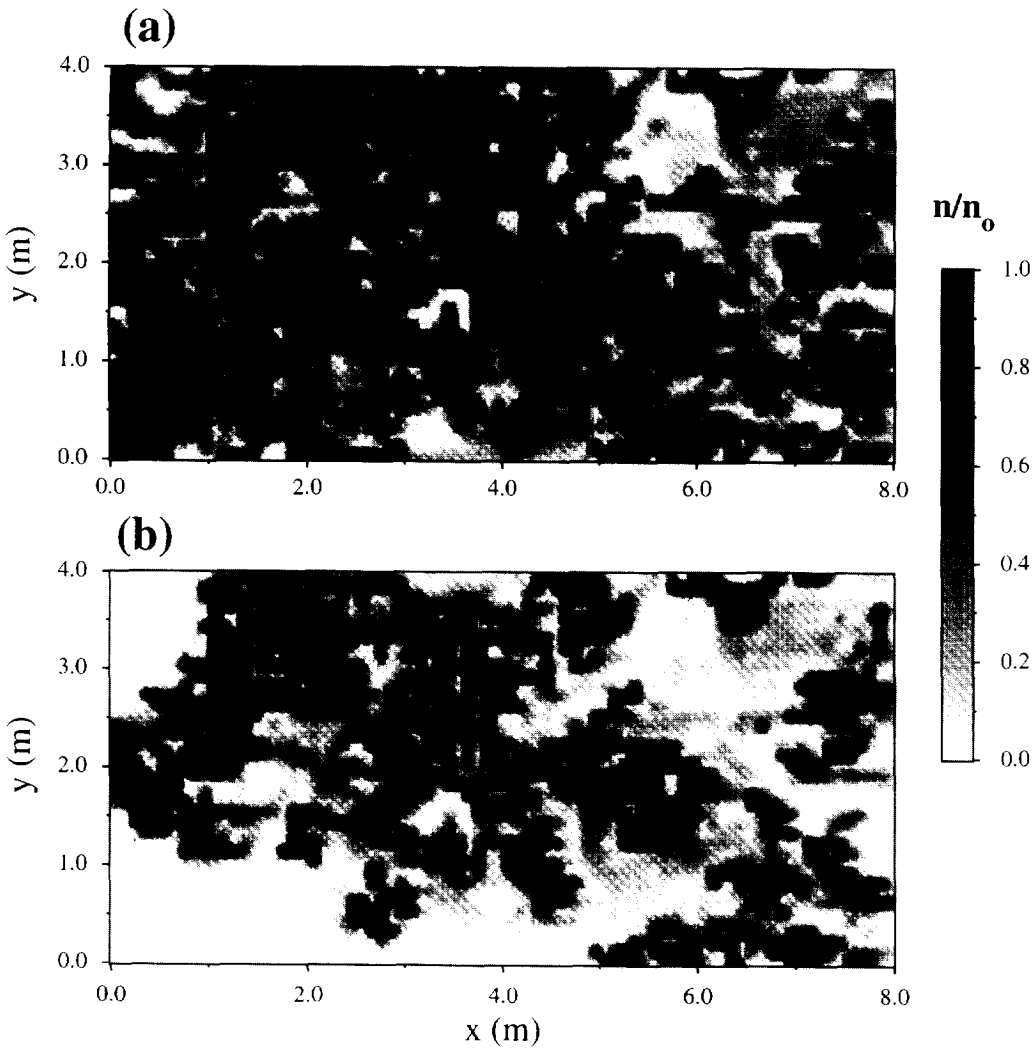

Fig. 2. Spatial distribution of normalized liquid-phase colloid concentration in the fracture plane for a colloid source uniformly distributed (a) across the entire width and (b) 1.0 m wide at the center of the inlet boundary. The gray scale illustrates normalized colloid concentrations ($t=10$ years, $d_p=1.0$ μm, $K=1.0\times10^{-8}$ m).

small aperture. This behavior is known as size exclusion, and is accounted for in this work by eliminating both the advective and dispersive fluxes onto fracture elements with apertures smaller than 12 times the colloidal particle diameter [16,40].

For every realization of the aperture field, the governing transport partial differential equation (Eq. (1)), coupled with either an equilibrium (Eq. (8)) or a kinetic (Eqs. (9)–(13)) colloid deposition model is solved numerically subject to initial and boundary conditions (Eqs. (3a), (3b), (3c), (3d) and (3e)) by employing the fully implicit finite-difference method, as outlined by Huyakorn and Pinder [17] and Strikwerda [48]. The time derivative is approximated by a two-point backward finite-difference scheme, and the spatial derivatives are approximated by a central finite-difference scheme. The overall approximation is second-order accurate. Unless otherwise indicated, the forward rate coefficient of the kinetic colloid deposition expression (Eq. (9)) is evaluated with a deposition coefficient $\kappa=1.0\times10^{-9}$ m [8]. For

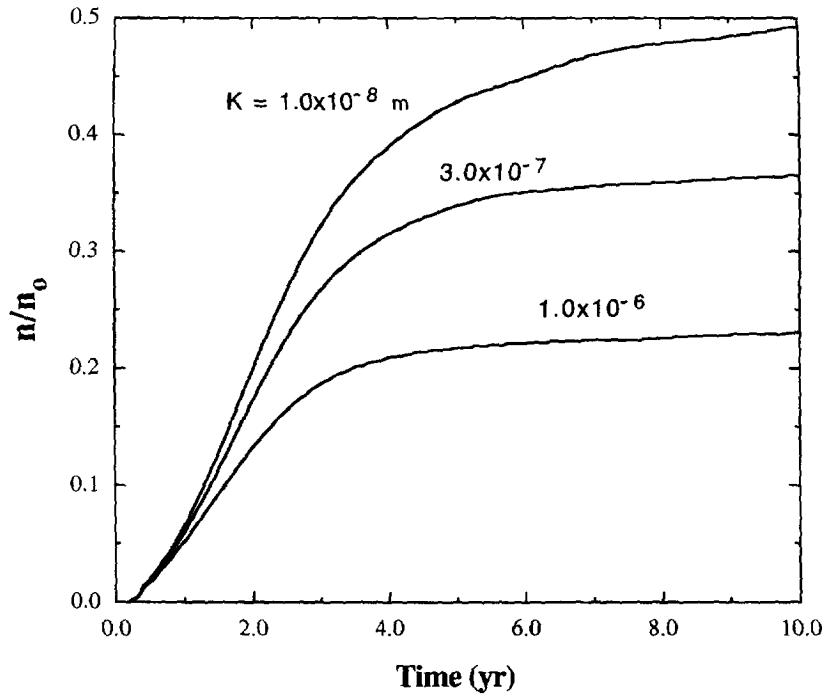

Fig. 3. Normalized ensemble-averaged temporal distribution of liquid-phase colloid concentration for equilibrium colloid deposition conditions and three different distribution coefficients ($d_p = 1.0$ μm, $x = 2.0$ m).

the estimation of other required colloid-deposition model parameters, it is assumed that $\rho_p = 2$ g cm^{-3} [24] and $\alpha = 15A_p$, or equivalently, $\beta = 15$ [47]; for $\beta = 15$ the value of the parameter k employed in Eq. (13) is approximately 0.033 [19].

It should be noted, however, that for a fracture with a spatially variable aperture the colloid deposition coefficient cannot be predicted in advance. Furthermore, the excluded-area factor can only be estimated from experimental colloid breakthrough curves [46]. Therefore, representative values for κ and β reported in the colloid literature are used for the colloid transport model simulations conducted in this study.

4. Simulations and discussion

4.1. Impact of equilibrium colloid deposition

For the case where colloid deposition is governed by the equilibrium relationship (Eq. (8)), snapshots of the liquid-phase colloid concentration in the fracture plane after ten years of simulation time are presented in Fig. 2 for two different colloid source conditions. In Fig. 2(a), the colloid source is distributed across the entire width of the fracture; whereas in Fig. 2(b), the colloid source is only 1 m wide at the center of the inlet boundary. Due to fracture-aperture variability and size exclusion, the observed colloid concentration distributions are non-uniform, and the existence of preferential transport is evident.

Colloid breakthrough curves for an ensemble average (i.e. expected value) of 60 aperture field realizations for different values of the distribution coefficient (K) are shown in Fig. 3. The curves represent averaged colloid concentrations across the fracture width at a distance of 2 m downstream from the inlet boundary. The number of realizations is selected so that results from additional realizations do not significantly alter the ensemble breakthrough curves. Fig. 3 indicates that increasing K leads to a lower liquid-phase colloid concen-

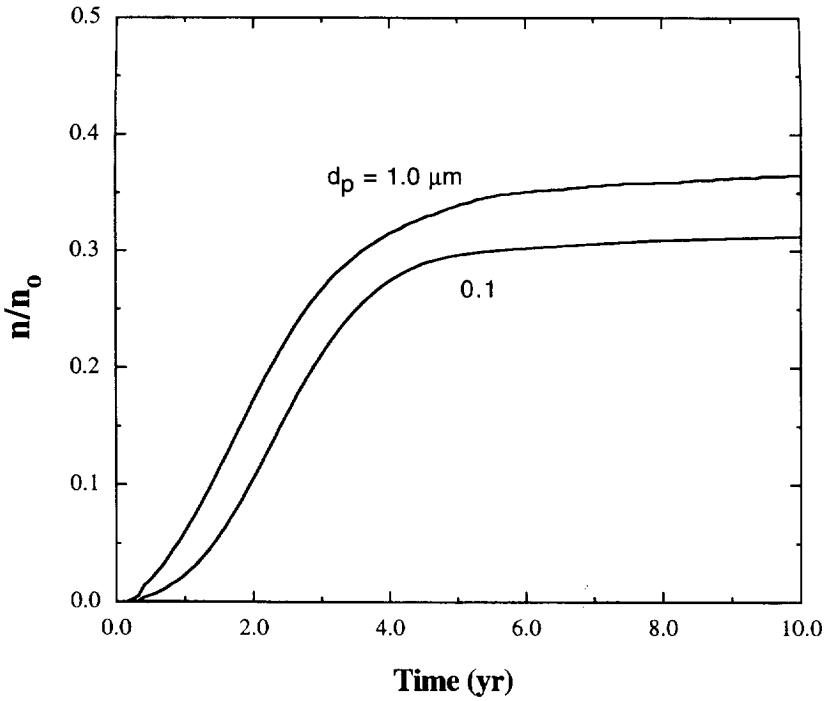

Fig. 4. Normalized ensemble-averaged temporal distribution of liquid-phase colloid concentration for equilibrium colloid deposition conditions and two different colloidal particle diameters ($K=3.0\times10^{-7}$ m, $x=2.0$ m).

tration. This is an expected result, because n^* increases with increasing K.

The effect of particle size on colloid transport in a saturated fracture with variable aperture under equilibrium deposition conditions is illustrated in Fig. 4. Colloid particles with diameters of 0.1 and 1.0 μm are considered for the same distribution coefficient. As the colloidal particle size gets smaller, the size exclusion effect becomes less important, because the number of elements in the fracture plane with an aperture smaller than 12 times the colloidal particle diameter is greatly reduced. Therefore, size exclusion contributes to the earlier breakthrough of colloids.

4.2. Impact of kinetic colloid deposition

4.2.1. Irreversible colloid deposition

When interstitial fluid and sorbent surface chemical conditions favor the presence of stable colloidal particles of opposite charge to sorbent surfaces, colloid deposition is essentially irreversible (i.e. $r_r=0$), and is restricted to monolayer coverage of sorbent surfaces [19]. For this case, Eq. (9) is employed with a zero reverse rate coefficient. Furthermore, the forward colloid deposition rate coefficient is defined by Eq. (10), and $F(n^*)$ is described either by a linear relationship (Eq. (11) or a non-linear model (Eq. (12) and Eq. (13).

Fig. 5 illustrates the effect of irreversible colloid deposition described by the linear DBF (Eq. (11)) on colloid transport for particles of 1.0 μm in diameter. The solid curves represent the clean-bed media assumption (i.e. $F(n^*)=1$) for which colloid deposition is unaffected by previously deposited particles [16], whereas the dashed curves represent the linear DBF. An ensemble average of 60 different realizations for a deposition coefficient of $\kappa=1.0\times10^{-9}$ m and a source colloid concentration distributed across the entire width of the inlet boundary is presented in Fig. 5(a). The rising portion of the two breakthrough curves in Fig. 5(a) coincide, because at early times the deposited colloid concentration is small ($\epsilon\rightarrow0$) and the linear

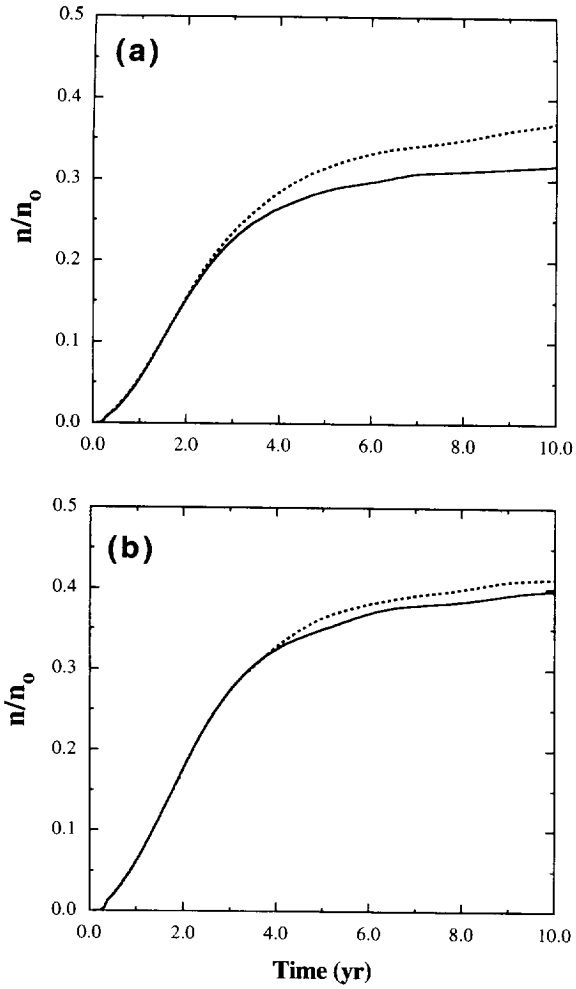

Fig. 5. Comparison between normalized ensemble-averaged temporal distribution of liquid-phase colloid concentration for irreversible colloid deposition conditions with linear DBF (dashed curves) and clean-bed media assumption (solid curves) for deposition coefficients of (a) $\kappa = 1.0 \times 10^{-9}$ m and (b) $\kappa = 5.0 \times 10^{-10}$ m ($d_p = 1.0$ μm, $x = 2.0$ m).

DBF is essentially 1. With increasing time, progressive deviation between the two curves is observed. As the portion of the fracture surface covered by deposited colloids increases ($\epsilon > 0$), the DBF decreases, and the rate of colloid deposition declines; consequently, the liquid-phase colloid concentration increases. In Fig. 5(b), a smaller deposition coefficient ($\kappa = 5.0 \times 10^{-10}$ m) is employed. Comparing Fig. 5(a) and Fig. 5(b), it is evident that the rising portion of the breakthrough curve for the linear DBF coincides with the curve corresponding to the case of $F(n^*) = 1$ for a longer period of time. At late times, the deviation of the breakthrough curves is less pronounced for the case of a smaller colloid deposition coefficient.

Fig. 6 presents breakthrough curves simulated for the same conditions as described in Fig. 5(a), with the exception that the diameter of the colloidal particles is an order of magnitude smaller ($d_p = 0.1$ μm). Comparison of Fig. 5(a) and Fig. 6 indicates that smaller colloidal particles require a longer period of time to break through due to weakening size exclusion effects, and yield higher liquid-phase colloid concentrations due to the reduction of the deposition rate. It should be noted that ϵ is inversely proportional to d_p (see Eq. (17)), and $F(n^*)$ decreases with increasing ϵ. Therefore, for invariant deposited colloid concentrations, a decrease in d_p leads to a reduction of both $F(n^*)$ and r_f, and ultimately to increased liquid-phase colloid concentrations.

The effect of the non-linear DBF presented in Eq. (12) and Eq. (13) on colloid transport is shown in Fig. 7. The solid curve represents the RSA DBF and the dashed curve the linear DBF. The source of colloids is located across the entire width of the fracture's inlet boundary. At early times, the rising portion of the two breakthrough curves is practically identical because the deposited colloid concentration is small. Consequently, the linear and non-linear DBFs are essentially equivalent. As the deposited colloid concentration increases, the RSA DBF yields higher liquid-phase colloid concentrations. Therefore, the colloid deposition rate is declining faster for the RSA DBF than for the linear DBF.

4.2.2. Reversible colloid deposition

In order to investigate the effect of the reverse rate coefficient on colloid transport, simulated breakthrough curves for an ensemble average of 60 realizations of the fracture aperture distribution, and for a source of colloids located across the entire width of the inlet boundary, is shown in Fig. 8(a) for $r_r = 1$ year^{-1}. The solid curve is for the case where the clean-bed media assumption is invoked, whereas the dashed curve is for the case where the linear DBF (Eq. (11)) is used. The non-

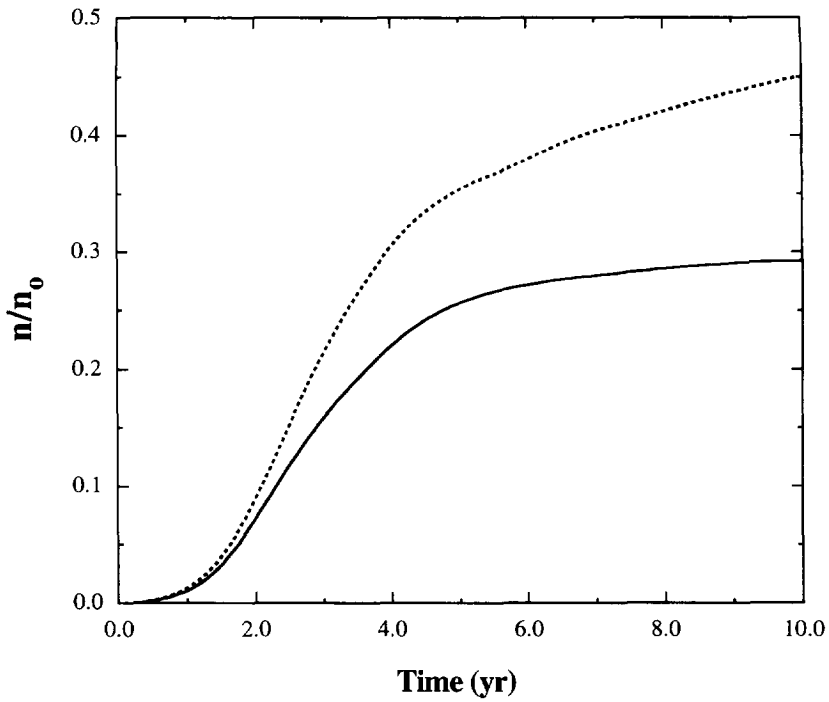

Fig. 6. Comparison between normalized ensemble-averaged temporal distribution of liquid-phase colloid concentration for irreversible colloid deposition conditions with linear DBF (dashed curve) and clean-bed media assumption (solid curve) for colloidal particles of 0.1 μm diameter ($\kappa = 1.0 \times 10^{-9}$ m, $x = 2.0$ m).

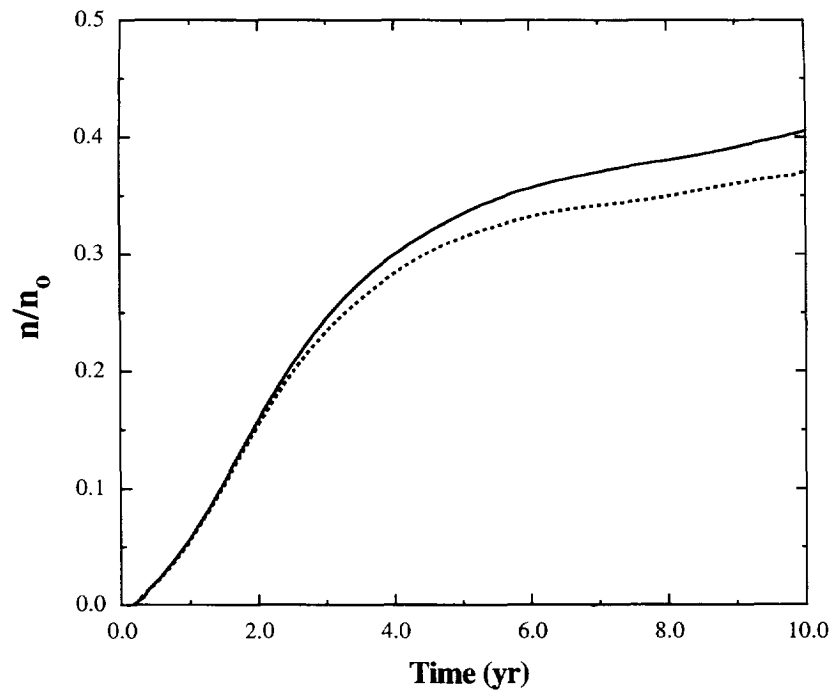

Fig. 7. Comparison between normalized ensemble-averaged temporal distribution of liquid-phase colloid concentration for irreversible colloid deposition conditions with linear DBF (dashed curve) and non-linear RSA DBF (solid curve) ($d_p = 1.0$ μm, $\kappa = 1.0 \times 10^{-9}$ m, $x = 2.0$ m).

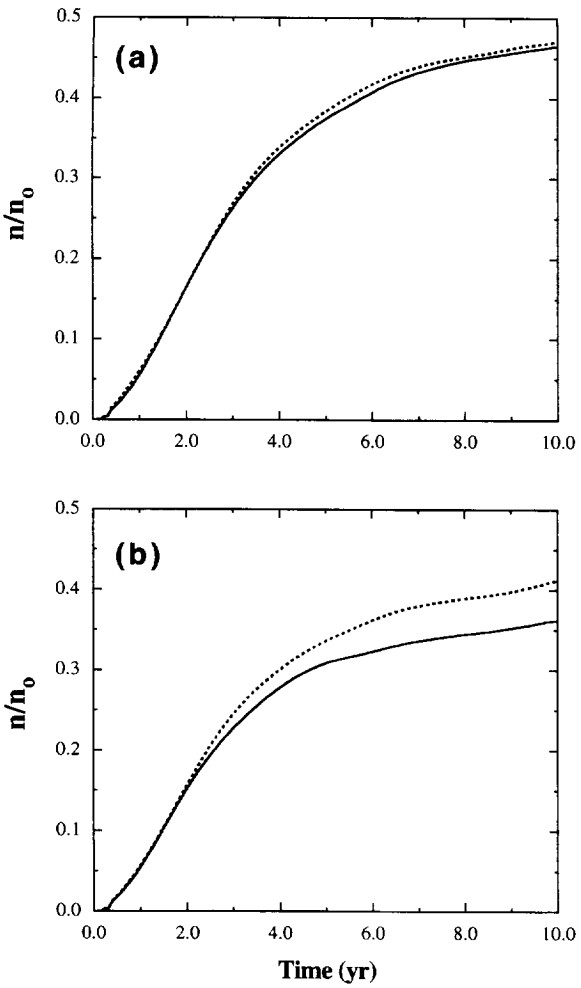

Fig. 8. Comparison between normalized ensemble-averaged temporal distribution of liquid-phase colloid concentration for reversible colloid deposition conditions with linear DBF (dashed curves) and clean-bed media assumption (solid curves) for reverse rate coefficients of (a) $r_r = 1.0$ year^{-1} and (b) $r_r = 0.1$ year^{-1} ($d_p = 1.0$ μm, $\kappa = 1.0 \times 10^{-9}$ m, $x = 2.0$ m).

linear RSA DBF is not employed because it accounts for only irreversible colloid deposition. The two breakthrough curves presented in Fig. 8(a) exhibit very similar behavior, because the effect of the linear DBF in decreasing the colloid deposition rate is insignificant due to the high reverse rate coefficient used, or equivalently, to the low deposited-colloid concentration. In Fig. 8(b), a reverse rate coefficient of $r_r = 0.1$ year^{-1} is used. Clearly, for this case the two breakthrough curves deviate progressively from each other with increasing time. The lower reverse-rate coefficient yields higher deposited-colloid concentrations. Consequently, the effect of the linear DBF in decreasing the colloid deposition rate is more pronounced due to increased coverage of fracture surfaces by previously deposited colloids.

5. Summary and conclusions

The transport of colloids in a spatially variable aperture is studied for equilibrium as well as kinetic colloid deposition conditions. Linear and non-linear dynamic blocking functions (DBFs) are examined for the case of kinetic colloid deposition. The colloid transport model developed accounts for size and surface exclusion, but neglects colloid diffusion into the rock matrix surrounding the fracture, because this effect is well documented in the literature to simply reduce the liquid-phase colloid concentration in the fracture. The governing partial differential equations are solved numerically using a fully implicit finite-difference scheme. Model simulations suggest that colloid spreading increases when fracture-aperture variability and size exclusion are considered, with the latter being important for large particles. Incorporating a DBF into the deposition model leads to higher liquid-phase colloid concentrations than those predicted by the clean-bed media assumption ($F(n^*) = 1$). The reason for this is that DBFs account for blocking effects from previously deposited colloidal particles. The non-linear DBF yields substantially higher liquid-phase colloid concentrations than the linear DBF, because the non-linear model declines faster with increasing deposited colloid concentration. The impact of the DBF in increasing the liquid-phase colloid concentration becomes insignificant at high reverse rate coefficients. Although the equilibrium colloid deposition mechanism is mathematically simple, it should be used with caution because it may not always represent accurately the colloid deposition process in subsurface systems.

Acknowledgment

Discussions with Terese M. Olson inspired this work. The preparation of the manuscript was supported in part by a UCI Faculty Career Development Award.

Appendix

List of symbols

A_p projected (cross-sectional) area of a colloidal particle: $\pi d_p^2/4$ (L^2)
b fracture aperture (L)
d_p diameter of a colloidal particle (L)
D_{ij} hydrodynamic dispersion coefficient in the ij ($ij = xx,xy,yx,yy$) direction ($L^2\,T^{-1}$)
$\boldsymbol{D}$ hydrodynamic dispersion coefficient tensor ($L^2\,T^{-1}$)
$\mathscr{D}$ Brownian diffusion coefficient ($L^2\,T^{-1}$)
F dynamic blocking function (–)
h total head potential in the fracture (L)
h_0 constant total head potential at the upstream boundary (L)
k empirical parameter which varies with α (–)
K partition coefficient for colloid deposition onto fracture surfaces (L)
K_f hydraulic conductivity of the fracture: $\gamma b^2/12\mu$ ($L\,T^{-1}$)
l_x fracture length in the x direction (L)
l_y fracture length in the y direction (L)
n colloid concentration in the liquid phase ($M\,L^{-3}$)
n_0 constant colloid concentration at the source ($M\,L^{-3}$)
n^* colloid concentration deposited on the fracture surfaces ($M\,L^{-2}$)
n^*_{max} maximum deposited colloid concentration on the fracture surfaces ($M\,L^{-2}$)
N^* number of colloidal particles per unit surface area of the fracture (L^{-2})
N^*_{max} maximum number of deposited colloids per unit surface area of the fracture (L^{-2})
r_f forward colloid deposition rate coefficient (T^{-1})
r_r reverse colloid deposition rate coefficient (T^{-1})
t time (T)
U_x interstitial velocity in the x direction ($L\,T^{-1}$)
U_y interstitial velocity in the y direction ($L\,T^{-1}$)
$\boldsymbol{U}$ interstitial velocity vector ($L\,T^{-1}$)
V_p volume of a spherical colloidal particle: $\pi d_p^3/6$ (L^3)
x coordinate along the fracture length (L)
y coordinate along the fracture width (L)

Greek letters

α fracture surface area blocked by a deposited colloidal particle (L^2)
α_L longitudinal dispersivity (L)
α_T transverse dispersivity (L)
β excluded area factor (–)
γ specific weight of the interstitial fluid ($M\,L^{-2}\,T^{-2}$)
δ_{ij} Kronecker delta
ϵ fraction of a fracture surface area covered (blocked) by deposited colloids (–)
ϵ_{max} fraction of a fracture surface area covered (blocked) by deposited colloids when n^* reaches n^*_{max} (–)
κ colloid deposition coefficient (L)
μ dynamic viscosity of the interstitial fluid ($M\,L^{-1}\,T^{-1}$)
ρ_p colloidal particle density ($M\,L^{-3}$)
∇ 2D vector operator (del): $\nabla = (\partial/\partial x, \partial/\partial y)^T$

Abbreviations

DBF dynamic blocking function
RSA random sequential adsorption

References

[1] A. Abdel-Salam and C.V. Chrysikopoulos, Adv. Water Res., 17 (1994) 283.
[2] A. Abdel-Salam and C.V. Chrysikopoulos, J. Hydrol., 165 (1995) 261.
[3] A. Abdel-Salam and C.V. Chrysikopoulos, Transport Porous Media, 20 (1995) 197.
[4] Z. Adamczyk, B. Siwek and M. Zembala, Colloids Surfaces, 62 (1992) 119.

[5] Z. Adamczyk, B. Siwek, M. Zembala and P. Belouschek, Adv. Colloid Interface Sci., 48 (1994) 151.
[6] A. Amirbahman and T.M. Olson, Colloids Surfaces A: Physicochem. Eng. Aspects, 95 (1995) 249.
[7] J. Bear and A. Verruijt, Modeling Groundwater Flow and Pollution, Reidel, Dordrecht, Holland, 1987.
[8] B.D. Bowen and N. Epstein, J. Colloid Interface Sci., 72 (1979) 81.
[9] R.W. Buddemeier and J.R. Hunt, Appl. Geochem., 3 (1988) 535.
[10] C.V. Chrysikopoulos and Y. Sim, J. Hydrol., 185 (1996) 199.
[11] G. de Marsily, Quantitative Hydrogeology: Groundwater Hydrology for Engineers, Academic Press, San Diego, CA, 1986.
[12] J.I. Drever, The Chemistry of Weathering, Reidel, Dordrecht, 1985.
[13] M. Elimelech, J. Gregory, X. Jia and R. Williams, Particle Deposition and Aggregation: Measurement, Modeling and Simulation, Butterworth-Heinemann, Oxford, 1995.
[14] P. Grindrod, J. Contam. Hydrol., 13 (1993) 167.
[15] S. Haber and H. Brenner, J. Colloid Interface Sci., 155 (1993) 226.
[16] J.P. Herzig, D.M. Leclerc and P. Le Goff, Ind. Eng. Chem., 62 (1970) 129.
[17] P.S. Huyakorn and G.F. Pinder, Computational Methods in Subsurface Flow, Academic Press, New York, NY, 1983.
[18] M. Ibaraki and E.A. Sudicky, Water Resour. Res., 31 (1995) 2945.
[19] P.R. Johnson and M. Elimelech, Langmuir, 11 (1995) 801.
[20] J.H. Kessler and J.R. Hunt, Water Resour. Res., 30 (1994) 1195.
[21] G.M. Litton and T.M. Olson, Environ. Sci. Technol., 27 (1993) 185.
[22] D. Liu, P.R. Johnson and M. Elimelech, Environ. Sci. Technol., 29 (1995) 2963.
[23] G. Matthess, A. Pekdeger and J. Schroeter, J. Contam. Hydrol., 2 (1988) 171.
[24] J.F. McCarthy and C. Degueldre, in J. Buffle and H.P. van Leeuwen (Eds.), Environmental Particles, Vol. 2, Lewis, Boca Raton, FL, 1993, p. 247.
[25] L.M. McDowell-Boyer, J.R. Hunt and N. Sitar, Water Resour. Res., 22 (1986) 1901.
[26] W.B. Mills, S. Liu, and F.K. Fong, Ground Water, 29 (1991) 199.
[27] V. Moulin and G. Ouzounian, Appl. Geochem. Suppl., 1 (1992) 179.
[28] Y. Ouyang, D. Shinde, R.S. Mansell and W. Harris, Crit. Rev. Environ. Sci. Technol., 26 (1996) 189.
[29] W.R. Penrose, W.L. Polzer, E.H. Essington, D.M. Nelson and K.A. Orlandini, Environ. Sci. Technol., 24 (1990) 228.
[30] Y. Pomeau, J. Phys. A: Math. Gen., 13 (1980) 193.
[31] V. Privman, H.L. Frisch, N. Ryde and E. Matijevic, J. Chem. Soc., Faraday Trans., 87 (1991) 1371.
[32] P.W. Reimus, B.A. Robinson, H.E. Nuttall and R. Kale, Mater. Res. Soc. Symp. Proc., 353 (1995) 363.
[33] E. Rodier and J. Dodds, Colloids Surfaces A: Physicochem. Eng. Aspects, 73 (1993) 77.
[34] W.B. Russel, D.A. Saville and W.R. Schowalter, Colloidal Dispersions, Cambridge University Press, Cambridge, 1989.
[35] J.N. Ryan and M. Elimelech, Colloids Surfaces A: Physicochem. Eng. Aspects, 107 (1996) 1.
[36] N. Ryde, N. Kallay and E. Matijevic, J. Chem. Soc., Faraday Trans., 87 (1991) 1377.
[37] N. Ryde, H. Kihira and E. Matijevic, J. Colloid Interface Sci., 151 (1992) 421.
[38] J.E. Saiers, G.M. Hornberger and L. Liang, Water Resour. Res., 30 (1994) 2499.
[39] J.E. Saiers, G.M. Hornberger and C. Harvey, J. Hydrol., 163 (1994) 271.
[40] R. Sakthivadivel, Clogging of a granular porous medium by sediment, Hydraulic Engineering Laboratory, University of California, Berkeley, Report HEL 15-17, 1969.
[41] P. Schaaf and J. Talbot, J. Chem. Phys., 91 (1989) 4401.
[42] Y. Sim and C.V. Chrysikopoulos, Water Resour. Res., 32 (1996) 1473.
[43] Y. Sim and C.V. Chrysikopoulos, Water Resour. Res., 32 (1996) 2607.
[44] P.A. Smith and C. Degueldre, J. Contam. Hydrol., 13 (1993) 143.
[45] I. Sojitra, K.T. Valsaraj, D.D. Reible and L.J. Thibodeaux, Colloids Surfaces A: Physicochem. Eng. Aspects, 110 (1996) 141.
[46] L. Song and M. Elimelech, Colloids Surfaces A: Physicochem. Eng. Aspects, 73 (1993) 49.
[47] L. Song and M. Elimelech, J. Colloid Interface Sci., 167 (1994) 301.
[48] J.C. Strikwerda, Finite Difference Schemes and Partial Differential Equations, Wadsworth and Brooks/Cole, Pacific Grove, CA, 1989.
[49] W. Stumm and J.J. Morgan, Aquatic Chemistry, 2nd ed. Wiley, New York, NY, 1981.
[50] S.W. Swanton, Adv. Colloid Interface Sci., 54 (1995) 129.
[51] U.S. Tim and S. Mostaghimi, Ground Water, 29 (1991) 251.
[52] L. Toran and A.V. Palumbo, J. Contam. Hydrol., 9 (1992) 289–303.
[53] T.G.M. van de Ven, Colloidal Hydrodynamics, Academic Press, London, 1989.
[54] S.A. Williams and A.I. El-Kadi, COVAR: A Computer Program for Generating Two-dimensional Fields of Autocorrelated Parameters by Matrix Decomposition, International Groundwater Modeling Center, Holcomb Research Institute, Colorado School of Mines, Golden, CO, 1986.